

Dynamics of 2023 FW₁₄, the second L₄ Mars trojan, and a physical characterization using the 10.4 m Gran Telescopio Canarias[★]

R. de la Fuente Marcos¹, J. de León^{2,3}, C. de la Fuente Marcos⁴, M. R. Alarcon^{2,3}, J. Licandro^{2,3}, M. Serra-Ricart^{2,3,5}, S. Geier^{6,2}, and A. Cabrera-Lavers^{6,2,3}

¹ AEGORA Research Group, Facultad de Ciencias Matemáticas, Universidad Complutense de Madrid, Ciudad Universitaria, E-28040 Madrid, Spain

² Instituto de Astrofísica de Canarias (IAC), C/ Vía Láctea s/n, E-38205 La Laguna, Tenerife, Spain

³ Departamento de Astrofísica, Universidad de La Laguna, E-38206 La Laguna, Tenerife, Spain

⁴ Universidad Complutense de Madrid, Ciudad Universitaria, E-28040 Madrid, Spain

⁵ Light Bridges S.L., Avda. Alcalde Ramírez Bethencourt, 17, E-35004, Las Palmas de Gran Canaria, Canarias, Spain

⁶ GRANTECAN, Cuesta de San José s/n, E-38712 Breña Baja, La Palma, Spain

Received 21 February 2024 / Accepted 4 March 2024

ABSTRACT

Context. Known Mars trojans could be primordial small bodies that have remained in their present-day orbits for the age of the Solar System. Their orbital distribution is strongly asymmetric; there are over a dozen objects at the L₅ point and just one at L₄, (121514) 1999 UJ₇. Most L₅ trojans appear to form a collision-induced asteroid cluster, known as the Eureka family. Asteroid 2023 FW₁₄ was recently discovered and it has a robust orbit determination that may be consistent with a Mars trojan status.

Aims. Our aim is determine the nature and dynamical properties of 2023 FW₁₄.

Methods. We carried out an observational study of 2023 FW₁₄ to derive its spectral class using the OSIRIS camera spectrograph at the 10.4 m Gran Telescopio Canarias. We investigated its possible trojan resonance with Mars using direct *N*-body simulations.

Results. The reflectance spectrum of 2023 FW₁₄ is not compatible with the olivine-rich composition of the Eureka family; it also does not resemble the composition of the Moon, although (101429) 1998 VF₃₁ does. The Eureka family and 101429 are at the L₅ point. The spectrum of 2023 FW₁₄ is also different from two out of the three spectra in the literature of the other known L₄ trojan, 121514, which are of C-type. The visible spectrum of 2023 FW₁₄ is consistent with that of an X-type asteroid, as is the third spectrum of 121514. Our calculations confirm that 2023 FW₁₄ is the second known L₄ Mars trojan although it is unlikely to be primordial; it may remain in its present-day “tadpole” path for several million years before transferring to a Mars-crossing orbit. It might be a fragment of 121514, but a capture scenario seems more likely.

Conclusions. The discovery of 2023 FW₁₄ suggests that regular Mars-crossing asteroids can be captured as temporary Mars trojans.

Key words. planets and satellites: individual: Mars – minor planets, asteroids: general – minor planets, asteroids: individual: 2023 FW₁₄ – techniques: spectroscopic – methods: numerical – celestial mechanics

1. Introduction

In the Solar System, trojans are small bodies that orbit the Sun engaged in a 1:1 mean-motion resonance with a planet, and therefore sharing the values of the orbital period of the planet and its semimajor axis, *a*. Jovian trojans are, for the most part, long-term stable and primordial (see, e.g., Levison et al. 1997; Holt et al. 2020); known Earth trojans are captured near-Earth asteroids and have unstable orbits (see, e.g., Connors et al. 2011; de la Fuente Marcos & de la Fuente Marcos 2021; Hui et al. 2021; Santana-Ros et al. 2022; Yeager & Golovich 2022). Dynamical studies suggest that some known Mars trojans could have remained in their present-day orbits for the age of the Solar System (see, e.g., Mikkola & Innanen 1994; Tabachnik & Evans 1999, 2000; Connors et al. 2005; Scholl et al. 2005; de la Fuente Marcos & de la Fuente Marcos 2013). Most L₅ Mars trojans are

believed to form a collision-induced asteroid cluster, called the Eureka family (Christou 2013; Christou et al. 2017).

Although the primordial nature of some of the known Mars trojans is still favored, alternative formation scenarios such as having been ejected from Mars due to a giant impact (Polishook et al. 2017) or resulting from rotational-fission via the thermal Yarkovsky-O’Keefe-Radzievskii-Paddack (YORP) mechanism (see, e.g., Ćuk et al. 2015; Christou et al. 2020) also agree with the available spectroscopy (see, e.g., Borisov et al. 2017). On the other hand, calculations by Schwarz & Dvorak (2012) suggest that present-day temporary capture of Mars trojans is possible.

The recently discovered Amor asteroid 2023 FW₁₄ (Chambers et al. 2023) follows an orbit that resembles those of known Mars trojans. Here we use reflectance spectroscopy and *N*-body simulations to determine the true nature of 2023 FW₁₄. This letter is organized as follows. In Sect. 2 we present the data and tools used in our analyses. In Sect. 3 we investigate whether 2023 FW₁₄ is a present-day Mars trojan and its origin and future dynamical evolution, and we derive its spectral class. In

Send offprint requests to: R. de la Fuente Marcos, e-mail: rauldefuentemarcos@ucm.es

[★] Based on observations made with the Gran Telescopio Canarias (GTC) telescope, in the Spanish Observatorio del Roque de los Muchachos of the Instituto de Astrofísica de Canarias (program ID GTC31-23A).

Table 1. Values of the heliocentric Keplerian orbital elements of 2023 FW₁₄ and their associated 1 σ uncertainties.

Orbital parameter	value \pm 1 σ uncertainty
Semimajor axis, a (au)	= 1.523769939 \pm 0.000000010
Eccentricity, e	= 0.15811207 \pm 0.00000010
Inclination, i ($^\circ$)	= 13.272714 \pm 0.000008
Longitude of the ascending node, Ω ($^\circ$)	= 21.84773 \pm 0.00002
Argument of perihelion, ω ($^\circ$)	= 245.29506 \pm 0.00004
Mean anomaly, M ($^\circ$)	= 26.03608 \pm 0.00003
Perihelion distance, q (au)	= 1.2828435 \pm 0.0000002
Aphelion distance, Q (au)	= 1.764696353 \pm 0.000000012
Absolute magnitude, H (mag)	= 21.6 \pm 0.4

Notes. The orbit determination of 2023 FW₁₄ is referred to epoch JD 2460200.5 (2023-Sep-13.0) TDB (Barycentric Dynamical Time, J2000.0 ecliptic and equinox), and is based on 47 observations with a data-arc span of 5503 d (solution date, April 22, 2023, 07:56:46 PDT). Source: JPL SBDB.

In Sect. 4 we discuss our results. Our conclusions are summarized in Sect. 5.

2. Data and tools

Object P21Es0a was found at $w=21.48$ mag by the Panoramic Survey Telescope and Rapid Response System (Pan-STARRS, Kaiser 2004; Denneau et al. 2013). The first reported observations were carried out by J. Bulger, T. Lowe, A. Schultz, and I. Smith on March 18, 2023, with the 1.8 m Pan-STARRS 2 Ritchey-Chretien telescope at Haleakala; on April 15, 2023, it was announced with the provisional designation 2023 FW₁₄ (Chambers et al. 2023). On April 19, 2023, a set of precoveries was released (Gray et al. 2023), leading to the orbit determination shown in Table 1 as retrieved from the Jet Propulsion Laboratory (JPL) Small-Body Database (SBDB)¹ provided by the Solar System Dynamics Group (SSDG, Giorgini 2011, 2015).²

The orbit determination shown in Table 1 is based on 47 observations with a data-arc span of 5503 d or 15.07 yr, and corresponds to a near-Earth asteroid (NEA) of the Amor dynamical class with moderate eccentricity, $e=0.158$, and inclination, $i=13.273^\circ$; however, its a value matches that of Mars at 1.524 au. The values of a and e automatically make 2023 FW₁₄ an object of interest regarding a possible resonant engagement with Mars. In terms of semimajor axis, Mars' co-orbital zone goes from ~ 1.51645 au to ~ 1.53095 au (see, e.g., Connors et al. 2005). Mars co-orbitals are expected to experience resonant behavior, temporary or long-term, if $e < 0.2$. Confirmation of a resonant engagement with Mars requires the analysis of results of N -body calculations. The orbit determination in Table 1 is referred to standard epoch JD 2460200.5 TDB, which is also the origin of time in the integrations presented here.

Most L₅ Mars trojans are thought to be part of an asteroid family. Asteroid family members are expected to have a common origin and composition. Surface mineralogy of asteroids is a proxy for their bulk composition; bodies with a common origin define tight clusters in orbital parameter space. The standard method used to study the surface mineralogy of asteroids is reflectance spectroscopy; the past and future orbital evolution of small bodies is explored using N -body simulations.

N -body simulations require orbit determinations and Cartesian state vectors as input data. In addition, and in order to provide reliable results, these calculations must take into account the uncertainties associated with the orbit determination (see, e.g., de la Fuente Marcos & de la Fuente Marcos 2018, 2020). For unstable chaotic dynamical evolution, the results have to be interpreted statistically. The calculations needed to study the possible resonant status with Mars of 2023 FW₁₄ were carried out using a direct N -body code developed by Aarseth (2003), publicly available from the web site of the Institute of Astronomy of the University of Cambridge.³ This software applies the Hermite numerical integration scheme devised by Makino (1991). Extensive results from this code were presented in de la Fuente Marcos & de la Fuente Marcos (2012).

Calculations were performed in an ecliptic coordinate system with the X -axis pointing toward the Vernal Equinox and in the ecliptic plane, the Z -axis perpendicular to the ecliptic plane and pointing northward, and the Y -axis orthogonal to the previous two and defining a right-handed coordinate system. Our physical model included the eight major planets, the Moon, the barycenter of the Pluto-Charon system, and the three largest asteroids. For accurate initial positions and velocities (see Appendix B), we used data from the JPL SSDG Horizons online Solar System data and ephemeris computation service,⁴ which are based on the DE440/441 planetary ephemeris (Park et al. 2021). Most input data were retrieved from JPL SBDB and Horizons using tools provided by the Python package Astroquery (Ginsburg et al. 2019) and its HorizonsClass class.⁵

The reflectance spectrum of 2023 FW₁₄ was interpreted by performing a taxonomical classification with the help of the Modeling for Asteroids (M4AST)⁶ online tool (Popescu et al. 2012). After applying a curve-fitting procedure to the spectrum, the tool makes a χ^2 comparison to the taxons defined by DeMeo et al. (2009) and provides the one with the lowest χ^2 .

3. Results

In this section we use reflectance spectroscopy and N -body simulations to investigate the surface mineralogy of 2023 FW₁₄ and its resonant status, probable origin, and future orbital evolution.

3.1. Spectroscopy

The visible spectrum of 2023 FW₁₄ was obtained on April 18, 2023, 21:12 UTC, using the Optical System for Imaging and Low Resolution Integrated Spectroscopy (OSIRIS) camera spectrograph (Cepa et al. 2000; Cepa 2010) at the 10.4 m Gran Telescopio Canarias (GTC), located at the El Roque de Los Muchachos Observatory (La Palma, Canary Islands). Observations were done under the program GTC31-23A (PI, J. de León). Appendix A details the instrumental setup and data reductions.

The resulting spectrum is shown in Fig. 1 (orange). The M4AST online tool provided a taxonomical classification as an Xc-type. For the sake of comparison, we also include the three visible spectra available in the literature of the other known L₄ Mars trojan, asteroid (121514) 1999 UJ₇: two spectra (in blue) from Borisov et al. (2018), obtained with the 4.2 m William Herschel Telescope (WHT, La Palma, Spain) and the 2 m Ritchey-Chretien-Coudé Telescope (2mRCC, Rozhen, Bulgaria), and a

³ <http://www.ast.cam.ac.uk/sverre/web/pages/nbody.htm>

⁴ <https://ssd.jpl.nasa.gov/horizons/>

⁵ <https://astroquery.readthedocs.io/en/latest/jplhorizons/jplhorizons.html>

⁶ <http://spectre.imcce.fr/m4ast/index.php/index/home>

¹ https://ssd.jpl.nasa.gov/tools/sbdb_lookup.html/#/

² <https://ssd.jpl.nasa.gov/>

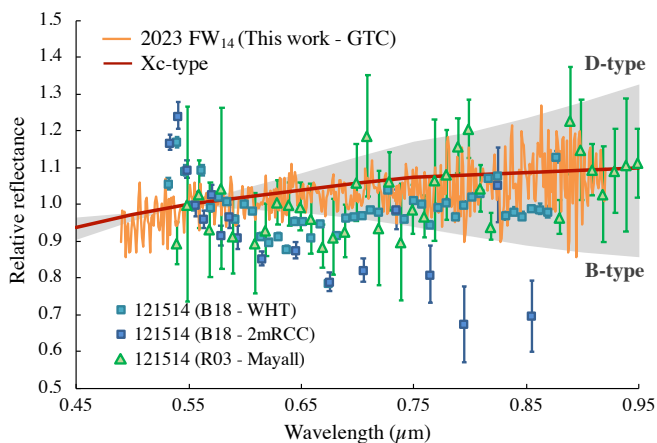


Fig. 1. Visible spectrum of 2023 FW₁₄ obtained with the 10.4 m GTC (in orange) and its best taxonomical match from the M4AST online tool, Xc-type (in red). The hatched gray area fills the entire domain between the mean B-type and D-type classes as defined by DeMeo et al. (2009). The blue squares correspond to two visible spectra published in Borisov et al. (2018) (labeled B18) of the other known L₄ Mars trojan, (121514) 1999 UJ₇. The third spectrum of 121514, shown here as green triangles, was published in Rivkin et al. (2003) (labeled R03).

third spectrum (in green) from Rivkin et al. (2003), obtained with the Mayall 4 m telescope (Kitt Peak, Arizona, USA). The third spectrum provides a taxonomical classification as an X-type, while the first spectrum provides a Ch-type classification. According to the authors the spectrum obtained with the 2mRCC telescope had a much poorer quality, and so was not used for classification.

Additional astrometry and photometric data were obtained with the Two-meter Twin Telescope (TTT), located at the Teide Observatory on the island of Tenerife (Canary Islands, Spain). These are two 0.80 m AltAz telescopes with f/4.4 and f/6.8, respectively. The observations were made using the QHY411M cameras (Alarcon et al. 2023) installed in one of the Nasmyth ports of both telescopes. The data collected served to improve the initial orbit determination.

3.2. Resonant status and orbital evolution

Trojans appear to move in what are called “tadpole” orbits (see, e.g., Murray & Dermott 1999) when viewed in a heliocentric frame of reference rotating with the host planet. For values of e and i close to zero, the tadpole trajectory has its center about 60° ahead of the host planet, around the Lagrange point L₄ (L₄ trojan), or follow 60° behind, around L₅ (L₅ trojan). In a general case, when the values of e and/or i are significant, the tadpole center may deviate from the standard $+60^\circ$ or -60° (or 300°) locations (see, e.g., Namouni & Murray 2000). In order to identify trojan resonant behavior, it is necessary to study the evolution of the relative mean longitude $\lambda_r = \lambda - \lambda_p$, where λ and λ_p are the mean longitudes of the trojan and the host planet, respectively; the relative mean longitude is given by $\lambda = M + \Omega + \omega$, where M is the mean anomaly, Ω is the longitude of the ascending node, and ω is the argument of perihelion (see, e.g., Murray & Dermott 1999). Only when the value of the critical angle, λ_r , oscillates or librates about $+60^\circ$ or -60° over an extended period of time, can the small body be classified as a trojan.

The orbit determination in Table 1 places 2023 FW₁₄ inside of the Mars co-orbital zone. Therefore, it may be co-orbital with

Mars; in other words, the value of λ_r may be librating instead of circulating in the interval $(0, 2\pi)$. Figure 2, top panel, shows the evolution of λ_r for the nominal orbit in Table 1; it displays more than one long period of its librational motion. The period of its L₄ trojan motion is 1350 yr, which is shorter than that of the other known L₄ trojan, (121514) 1999 UJ₇, 1500 yr, but similar to those of most known L₅ trojans (de la Fuente Marcos & de la Fuente Marcos 2013). Its amplitude is 33° , which is smaller than that of 121514, 77° , and (101429) 1998 VF₃₁, 45° , but larger than those of 5261 Eureka, 11° ; (385250) 2001 DH₄₇, 11° ; (311999) 2007 NS₂, 14° ; 2011 SC₁₉₁, 18° ; 2011 SL₂₅, 18° ; and 2011 UN₆₃, 14° (de la Fuente Marcos & de la Fuente Marcos 2013). The value of λ_r oscillates around $+66^\circ$ instead of $+60^\circ$ because the orbit of 2023 FW₁₄ is somewhat eccentric and inclined. Figure 2, bottom panel, shows the associated tadpole loop in the coordinate system corotating with Mars. The tadpole loop is the result of the superposition of multiple short-period epicyclic loops reflecting the motion of the trojan relative to Mars. Our short-term integrations of the nominal orbit confirm that 2023 FW₁₄ moves in the vicinity of the Mars Lagrange point L₄. Its motion about the equilateral libration point ahead of Mars is consistent with trojan dynamical behavior. However, the orbit determination in Table 1 is affected by uncertainties, and we must show that the evolution of λ_r of any orbit statistically consistent with the observational data leads to trojan behavior as well.

Figure 3, top panel, shows the evolution of λ_r for the nominal orbit and those of relevant control orbits or clones. The evolution is virtually identical for all the control orbits within $\pm 9\sigma$ of the nominal orbit determination in Table 1, but the bottom panel shows that when considering the differences in the values of λ_r with respect to the nominal values, some variation exists. In any case, consistent trojan behavior was found for all the control orbits within $\pm 9\sigma$ of the nominal orbit determination (1000 were integrated). Therefore, we conclude that 2023 FW₁₄ is the second known L₄ Mars trojan. However, most of the previously known Mars trojans appear to be stable over the age of the Solar System (see, e.g., de la Fuente Marcos & de la Fuente Marcos 2013). Longer integrations are needed to investigate whether 2023 FW₁₄ is just a temporary trojan or long-term stable.

Figure 4 shows the evolution of λ_r for the nominal orbit and those of relevant control orbits for longer integrations. The evolution of λ_r confirms that 2023 FW₁₄ is not a long-term stable L₄ Mars trojan. It also shows that the evolution of this temporary trojan is far more unstable when considering its past. The object only became an L₄ Mars trojan nearly 1 Myr ago and it will leave its current trojan engagement with Mars perhaps as early as 13 Myr from now. The most straightforward interpretation of these results is that it might have been captured from the population of Mars-crossing NEAs and will return to it after escaping Mars’ co-orbital region. Although all the control orbits became trojans at about the same time when integrated backward in time, there is a considerable dispersion in the results of forward integrations (although the evolutions of 7 orbits are shown, 25 were studied). We can conclude with certainty that 2023 FW₁₄ is not a long-term stable L₄ Mars trojan, but we cannot provide a reliable prediction of the exact duration of the current trojan episode beyond stating that it will last more than 10 Myr. Therefore, it is unlikely to be primordial.

4. Discussion

Among L₄ Mars trojans, 2023 FW₁₄ has the highest orbital eccentricity (0.158) and the lowest inclination (13.273°). This

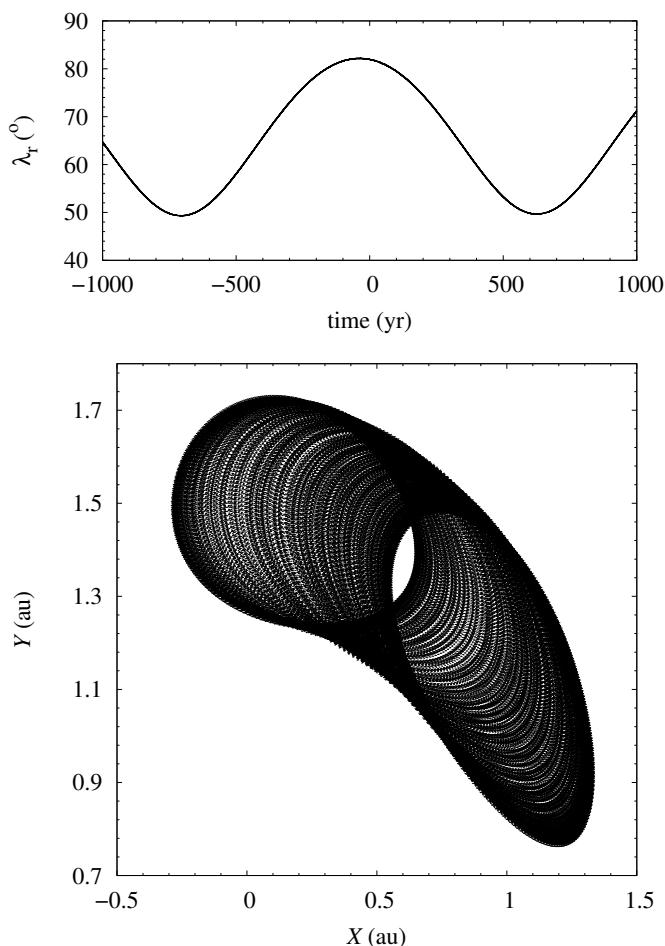


Fig. 2. Resonant behavior of 2023 FW₁₄. *Top panel:* Evolution of the relative mean longitude for the nominal orbit of 2023 FW₁₄ in the time interval (−1000, 1000) yr. *Bottom panel:* Tadpole loop in the coordinate system corotating with Mars (Sun–Mars rotating frame) corresponding to the same time interval; tadpole loops are made of multiple overlapping epicyclic loops. The output time-step size is 0.01 yr.

value of i places 2023 FW₁₄ inside the unstable region identified by Scholl et al. (2005) where various secular resonances will remove a trojan within a few million years. In addition, it has the largest value of H (21.6 mag). NEOWISE observations of (121514) 1999 UJ₇ (Nugent et al. 2016) provide a value of its visible albedo of 0.047 ± 0.023 , which is compatible with its classification as an X-type asteroid by Rivkin et al. (2003). Using this value of the albedo and the absolute magnitude in Table 1, we derive a mean diameter of $D = 318^{+493}_{-199}$ m for 2023 FW₁₄. If the only other L₄ Mars trojan, 121514, is the largest known Mars trojan, then 2023 FW₁₄ could be one of the smallest known so far.

In principle, the long-term behavior into the past of 2023 FW₁₄ is compatible with capture from the population of Mars-crossing NEAs, but an origin as a fragment of another trojan, either known or still undiscovered, cannot be discarded considering the available data. Our calculations indicate that the evolution of 2023 FW₁₄ is stable for over 10 Myr; this is much shorter than the stability timescale of the other trojans, but also significantly longer than the typical duration of the resonant episodes of transient Mars co-orbitals discussed by Connors et al. (2005). This might be hinting at an in situ origin for 2023 FW₁₄. Regarding the provenance of 121514, it has been

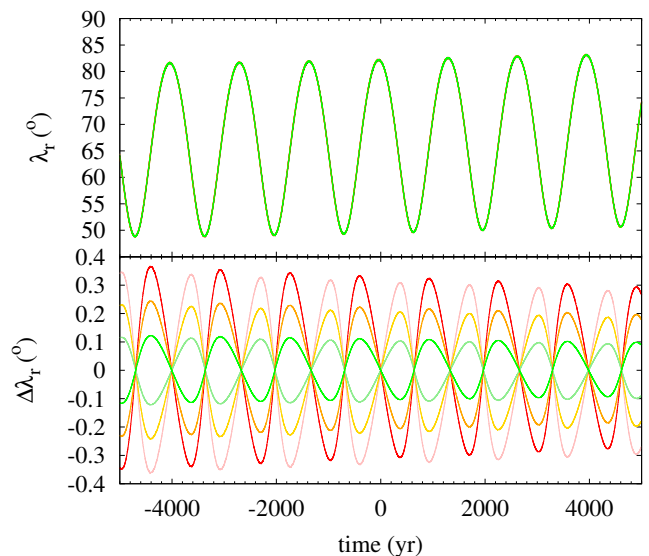


Fig. 3. Uncertainties and resonant behavior of 2023 FW₁₄. *Top panel:* Evolution of the relative mean longitude with Mars for the nominal orbit (in black) of 2023 FW₁₄ and those of relevant control orbits in the time interval (−5 000, 5 000) yr. The control orbits or clones have Cartesian state vectors (see Appendix B) separated $+3\sigma$ (green), -3σ (light-green), $+6\sigma$ (orange), -6σ (gold), $+9\sigma$ (red), and -9σ (pink) from the nominal values in Table B.1. *Bottom panel:* Evolution of the difference between the value of the λ_T of the control orbits and that of the nominal orbit for the same time interval. The output time-step size is 0.1 yr.

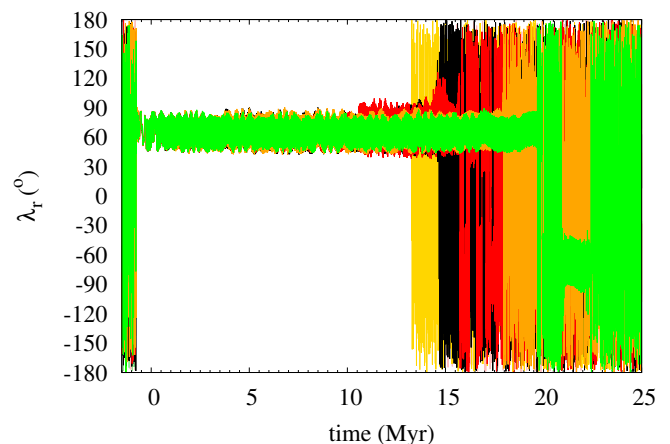


Fig. 4. Long-term resonant behavior of 2023 FW₁₄. Evolution of the relative mean longitude with Mars for the nominal orbit (in black) of 2023 FW₁₄ and those of relevant control orbits in the time interval (−1.5, 25.0) Myr. The control orbits or clones have Cartesian state vectors (see Appendix B) separated $+3\sigma$ (in green), -3σ (in light-green), $+6\sigma$ (in orange), -6σ (in gold), $+9\sigma$ (in red), and -9σ (in pink) from the nominal values in Table B.1. The output time-step size is 5 000 yr.

suspected that this trojan is not primordial, but it was captured about 4 Gyr ago (de la Fuente Marcos & de la Fuente Marcos 2013). Another probable captured trojan is (101429) 1998 VF₃₁ (de la Fuente Marcos & de la Fuente Marcos 2013). Spectroscopic results also argue for a different origin in the case of 101429 and 121514 (Rivkin et al. 2007; Christou et al. 2021).

The second hypothesis regarding the origin of 2023 FW₁₄ can be partially tested using the spectroscopic information. The reflectance spectrum of 2023 FW₁₄ is neither compatible with an olivine-rich composition like that of the Eureka family (Borisov

et al. 2017) nor resembles the one of the Moon, like in the case of 101429 (Christou et al. 2021), both at L₅. It is on the contrary a primitive-like spectrum, matching the Xc-type class. There are three spectra in the literature for the other known L₄ trojan, asteroid 121514. The spectrum obtained by Borisov et al. (2018) with the 4.2 m WHT yields a Ch-type classification, mainly due to the presence of a broad absorption feature centered at $\sim 0.64\text{--}0.65\ \mu\text{m}$. However, neither the center nor the shape of this absorption is typical of the 0.7 μm absorption observed in Ch-type asteroids and associated with phyllosilicates. Even the authors note this point and invoke a potential new subclass of the C-complex to explain this spectrum. The other spectrum of 121514, classified as an X-type, was obtained by Rivkin et al. (2003). All in all, and even considering the poorer quality of the data previously obtained for 121514 compared to our spectrum of 2023 FW₁₄, we can confidently say that these two asteroids have primitive-like spectra, in contrast with the trojans studied in L₅. Although incomplete, the data support the interpretation of 2023 FW₁₄ as an interloper captured from the Mars-crossing NEA population, but they cannot be used to reject the competing hypothesis that 2023 FW₁₄ was produced in situ by, for example, YORP-induced rotational fission, as perhaps in the case of the Eureka family (Ćuk et al. 2015; Christou et al. 2020) because the spectra of 121514 and 2023 FW₁₄ are somewhat close (see Fig. 1). On the other hand, and although the present-day 121514 is a slow rotator (Borisov et al. 2018) and therefore not capable of shedding material via the YORP mechanism, its spin state might have been different in the past (Christou et al. 2020).

5. Summary and conclusions

In this letter we presented spectroscopic observations of Mars' second L₄ trojan, 2023 FW₁₄, obtained on April 18, 2023, using the OSIRIS camera-spectrograph at the 10.4 m GTC. We used the spectrum to provide a physical characterization of the object and direct *N*-body simulations to confirm its trojan resonant state and investigate its orbital evolution. Our conclusions can be summarized as follows:

1. We find that 2023 FW₁₄ has a visible spectrum consistent with that of an Xc-type asteroid.
2. We confirm that 2023 FW₁₄ is the second known L₄ Mars trojan.
3. We confirm that 2023 FW₁₄ is a temporary L₄ Mars trojan that might have been captured from the Mars-crossing NEA population about 1 Myr ago or, less likely, shed from (121514) 1999 UJ₇. Its current trojan episode will last at least 10 Myr.

Schwarz & Dvorak (2012) found that the present-day temporary capture of Mars trojans is possible. The discovery of 2023 FW₁₄ could be the confirmation of this theoretical possibility.

Acknowledgements. We thank the anonymous referee for a prompt and helpful report, and S. Deen for finding precovery images of 2023 FW₁₄ that improved the orbital solution of this object significantly and for additional comments. RdlFM and CdIFM thank S. J. Aarseth for providing one of the codes used in this research and A. I. Gómez de Castro for providing access to computing facilities. JdL and JL acknowledge financial support from the Spanish Ministry of Science and Innovation (MICINN) through the Spanish State Research Agency, under Severo Ochoa Programme 2020-2023 (CEX2019-000920-S). This work was partially supported by the Spanish 'Agencia Estatal de Investigación (Ministerio de Ciencia e Innovación)' under grant PID2020-116726RB-I00/AEI/10.13039/501100011033. Based on observations made with the Gran Telescopio Canarias (GTC), installed at the Spanish Observatorio del Roque de los Muchachos of the Instituto de Astrofísica de Canarias, on the island of La Palma. This work is partly based on data obtained with the instrument OSIRIS,

built by a Consortium led by the Instituto de Astrofísica de Canarias in collaboration with the Instituto de Astronomía de la Universidad Nacional Autónoma de México. OSIRIS was funded by GRANTECAN and the National Plan of Astronomy and Astrophysics of the Spanish Government. This letter includes observations made with the Two-meter Twin Telescope (TTT) at the IAC's Teide Observatory that Light Bridges, SL, operates on the Island of Tenerife, Canary Islands (Spain). The Observing Time Rights (DTO) used for this research at the TTT have been provided by the Instituto de Astrofísica de Canarias. In preparation of this letter, we made use of the NASA Astrophysics Data System, the ASTRO-PH e-print server, and the MPC data server.

References

- Aarseth, S. J. 2003, *Gravitational N-Body Simulations* (Cambridge: Cambridge University Press), 27
- Alarcon, M. R., Licandro, J., Serra-Ricart, M., et al. 2023, *PASP*, 135, 055001
- Borisov, G., Christou, A., Bagnulo, S., et al. 2017, *MNRAS*, 466, 489
- Borisov, G., Christou, A. A., Colas, F., et al. 2018, *A&A*, 618, A178
- Cepa, J., Aguiar, M., Escalera, V. G., et al. 2000, *Proc. SPIE*, 4008, 623
- Cepa, J. 2010, *Astrophysics and Space Science Proceedings*, 14, 15
- Chambers, K., Chastel, S., de Boer, T., et al. 2023, *Minor Planet Electronic Circulars*, 2023-G87
- Christou, A. A. 2013, *Icarus*, 224, 144
- Christou, A. A., Borisov, G., Dell'Oro, A., et al. 2017, *Icarus*, 293, 243
- Christou, A. A., Borisov, G., Dell'Oro, A., et al. 2020, *Icarus*, 335, 113370
- Christou, A. A., Borisov, G., Dell'Oro, A., et al. 2021, *Icarus*, 354, 113994
- Connors, M., Wiegert, P., & Veillet, C. 2011, *Nature*, 475, 481
- Connors, M., Stacey, G., Brasser, R., et al. 2005, *Planet. Space Sci.*, 53, 617
- Ćuk, M., Christou, A. A., & Hamilton, D. P. 2015, *Icarus*, 252, 339
- de la Fuente Marcos, C. & de la Fuente Marcos, R. 2012, *MNRAS*, 427, 728
- de la Fuente Marcos, C. & de la Fuente Marcos, R. 2013, *MNRAS*, 432, L31
- de la Fuente Marcos, C. & de la Fuente Marcos, R. 2018, *MNRAS*, 473, 2939
- de la Fuente Marcos, C. & de la Fuente Marcos, R. 2020, *MNRAS*, 494, 1089
- de la Fuente Marcos, C. & de la Fuente Marcos, R. 2021, *RNAAS*, 5, 29
- DeMeo, F., Binzel, R. P., Slivan, S. M., et al. 2009, *Icarus*, 202, 160
- Denneau, L., Jedicke, R., Grav, T., et al. 2013, *PASP*, 125, 357
- Ginsburg, A., Sipőcz, B. M., Brasseur, C. E., et al. 2019, *AJ*, 157, 98
- Giorgini, J. 2011, in *Journées Systèmes de Référence Spatio-temporels 2010*, ed. N. Capitaine, 87–87
- Giorgini, J. D. 2015, *IAUGA*, 22, 2256293
- Gray, B., Rankin, D., Shelly, F. C., et al. 2023, *Minor Planet Electronic Circulars*, 2023-H105
- Holt, T. R., Nesvorný, D., Horner, J., et al. 2020, *MNRAS*, 495, 4085
- Hui, M.-T., Wiegert, P. A., Tholen, D. J., et al. 2021, *ApJ*, 922, L25
- Kaiser, N. 2004, *Proc. SPIE*, 5489, 11
- Levison, H. F., Shoemaker, E. M., & Shoemaker, C. S. 1997, *Nature*, 385, 42
- Licandro, J., de la Fuente Marcos, C., de la Fuente Marcos, R., et al. 2019, *A&A*, 625, A133
- Makino, J. 1991, *ApJ*, 369, 200
- Mikkola, S. & Innanen, K. 1994, *AJ*, 107, 1879
- Murray, C. D., & Dermott, S. F. 1999, *Solar System Dynamics* (Cambridge: Cambridge University Press)
- Namouni, F. & Murray, C. D. 2000, *Celestial Mechanics and Dynamical Astronomy*, 76, 131
- Nugent, C. R., Mainzer, A., Bauer, J., et al. 2016, *AJ*, 152, 63
- Park, R. S., Folkner, W. M., Williams, J. G., et al. 2021, *AJ*, 161, 105
- Polishook, D., Jacobson, S. A., Morbidelli, A., et al. 2017, *Nature Astronomy*, 1, 0179
- Popescu, M., Birlan, M., & Nedelcu, D. A. 2012, *A&A*, 544, A130
- Rivkin, A. S., Binzel, R. P., Howell, E. S., et al. 2003, *Icarus*, 165, 349
- Rivkin, A. S., Trilling, D. E., Thomas, C. A., et al. 2007, *Icarus*, 192, 434
- Santana-Ros, T., Micheli, M., Faggioli, L., et al. 2022, *Nat. Commun.*, 13, 447
- Scholl, H., Marzari, F., & Tricarico, P. 2005, *Icarus*, 175, 397
- Schwarz, R. & Dvorak, R. 2012, *Celestial Mechanics and Dynamical Astronomy*, 113, 23
- Tabachnik, S. & Evans, N. W. 1999, *ApJ*, 517, L63
- Tabachnik, S. A. & Evans, N. W. 2000, *MNRAS*, 319, 63
- Yeager, T. & Golovich, N. 2022, *ApJ*, 938, 9

Table B.1. Barycentric Cartesian state vector of 2023 FW₁₄: components and associated 1 σ uncertainties.

Component	value $\pm 1\sigma$ uncertainty
X (au)	$= 6.915652422725076 \times 10^{-1} \pm 4.45004793 \times 10^{-7}$
Y (au)	$= -1.076839004164107 \times 10^{+0} \pm 3.69180966 \times 10^{-7}$
Z (au)	$= -2.965493352209987 \times 10^{-1} \pm 1.79345340 \times 10^{-7}$
V_X (au/d)	$= 1.411478671143701 \times 10^{-2} \pm 1.85662865 \times 10^{-9}$
V_Y (au/d)	$= 7.479403282969601 \times 10^{-3} \pm 4.72439409 \times 10^{-9}$
V_Z (au/d)	$= 4.005959201684231 \times 10^{-4} \pm 1.69044868 \times 10^{-9}$

Notes. Data are referred to epoch JD 2460200.5, which corresponds to 0:00 on 2023-Sep-13.0 TDB (J2000.0 ecliptic and equinox). Source: JPL Horizons.

Appendix A: Spectroscopic observations and data reduction

We used the OSIRIS camera-spectrograph at the 10.4 m GTC. The OSIRIS detector is a blue-sensitive monolithic 4096 \times 4096 pixel CCD that provides an unvignetted field of view of 7.8' \times 7.8'. The standard operation mode of the instrument uses a 2 \times 2 binning. We used the R300R grism that covers a wavelength range from 0.48 to 0.92 μ m, with a dispersion of 7.74 \AA /pixel for a 0.6" slit. We used the 1.2" slit, oriented to the parallactic angle, and with the tracking of the telescope at a set rate matching the proper motion of the asteroid. We obtained three consecutive spectra of 900 s of exposure time each, at an airmass of 1.3, offsetting the telescope 10" in the slit direction between the spectra. To obtain the reflectance spectra of the asteroid, we also observed two solar analog stars (Landolt SA 98-978 and SA 102-1081), using the same instrumental configuration as for the asteroid, and at a similar airmass. In the case of the stars, we obtained three individual spectra, also offsetting the telescope in the slit direction by 10" between individual spectra. Spectral images of the asteroid and the solar analog stars were bias and flat-field corrected. The 2D spectra were background subtracted and collapsed to 1D by adding all the flux within an aperture (typically defined as the distance from the center of the spatial profile where the intensity is 10% of the peak intensity). One-dimensional spectra were then wavelength calibrated using Xe+Ne+HgAr arc lamps. We added the three asteroid spectra, and averaged, for each solar analog, the corresponding individual spectra. Then, as a final step, we divided the spectrum of the asteroid by the spectrum of each solar analog star, and averaged the two resulting ratios. This final spectrum is shown in Fig. 1 in orange. Additional details are described in Licandro et al. (2019), among others.

Appendix B: Input data

Here, we include the barycentric Cartesian state vector of L₄ Mars trojan 2023 FW₁₄. This vector and its uncertainties have been used to perform the calculations discussed in the sections and to generate the figures that display the time evolution of the critical angle, λ_c . For example, a new value of the X -component of the state vector is computed as $X_c = X + \sigma_X r$, where r is an univariate Gaussian random number, and X and σ_X are the mean value and its 1 σ uncertainty from Table B.1.